Rutherford backscattering from a thick target

Ž. Šmit
J. Stefan Institute, University of Ljubljana, Ljubljana, Slovenia
(Received 24 March 1993)

The plural- and multiple-scattering contribution to the thick-target Rutherford backscattering (RBS) yield was calculated as a part of the single-scattering yield. The method is based on an approximation of the finite total scattering cross section and employs Poisson statistics for the number of collisions along the ionic trajectory. Within a linear approximation, trajectories with different numbers of collisions contribute to the total scattering yield in a way similar to the double-scattering process. The resulting total scattering yield is expressed as a multiple of the single-scattering one, and is suitable for applications in RBS spectroscopy. The validity of the model is limited to systems of light projectiles and heavy targets, to backscattering angles close to 180°, and to the high-energy part of the spectra.

PACS number(s): 79.20.Nc, 61.80.Mk, 34.50.Bw

I. INTRODUCTION

When thick targets are used for a Rutherford-backscattering (RBS) experiment, the scattered ions exhibit a characteristic energy distribution due to stopping in the target. For a sufficiently thick target, the energy spectrum of the scattered ions extends from zero up to the impact energy E_1, reduced by a kinematic factor k. In the simplest model, the spectral shape is explained as a result of the single-scattering events [1]. The ion path is assumed to be a straight line, broken by the respective scattering atom in the target. The validity of this model is limited to the near-surface region of the target. For the inner parts, plural and multiple scattering provides a significant contribution to the single-scattering spectrum, enhancing its low-energy part. For 0.1-MeV protons impinging on a gold target, the spectral shape was well reproduced by the Monte Carlo simulation of Steinbauer *et al.* [2–4]. For applications in RBS spectrometry, an analytical expression for the thick-target yield is of great practical importance. Thick-target scattering has been treated analytically by Sirotinin and co-workers [5–7]. The authors assumed that the ions attain a well peaked angular distribution before and after the principal (large-angle) scattering. The plural- and multiple-scattering correction to the RBS spectrum was obtained as a simple multiplicative factor which depends merely on the angular spreads of ions before and after the principal scattering. In the present study, the factor of Sirotinin and co-workers was found to reproduce about one half of the plural- and multiple-scattering yield. In the Monte Carlo calculations [2–4], the authors distinguished between the ion trajectories with one, two, and any particular number of collisions. A similar model was used here, but it is largely based on the symmetry properties of the Legendre polynomials as a function of the ion deflection angle. An improved expression for the total scattering yield is derived.

II. THEORY

A. The scattering cross section

In the center of mass system, the Rutherford cross section on a bare nucleus can be written in the form

$$\frac{d\sigma}{d\Omega} = \frac{d^2(E)}{(1-\cos\vartheta)^2}, \tag{1}$$

where ϑ is the scattering angle and $d(E)$ is one-half of the distance for the head on collision at the energy E. Screening of atomic electrons substantially reduces the cross section for low scattering angles. Several approximations were used to describe this effect.

(a) Goudsmit and Saunderson [8] proposed to set $\frac{d\sigma}{d\Omega}$ to zero for scattering angles smaller than a certain scattering angle ϑ_c. Consequently, scattering occurs for impact parameters smaller than the cutoff radius $a_c = d\cot\frac{\vartheta_c}{2}$.

(b) Wentzel [9] calculated $\frac{d\sigma}{d\Omega}$ in a Born approximation for the Coulomb potential multiplied by an exponential screening function. A result similar to (1) was obtained, but with the denominator in (1) replaced by $(1+r-\cos\vartheta)^2$, where r is a small positive constant (not specified here). The parameter r unimportantly influences $\frac{d\sigma}{d\Omega}$ at large scattering angles. The calculation was also performed numerically for the Thomas-Fermi potential [8].

(c) For small impact energies used in RBS experiments, scattering is classical. Güttner [10] and Andersen *et al.* [11] expanded the screening function up to the first order term, cut off the potential in the region of an opposite sign, and solved analytically the classical scattering integral. The result is similar to that of Wentzel, but with a different parameter r. Again, scattering only occurs for impact parameters smaller than a_c, which for the Thomas-Fermi screening function is given by $0.63a_F$ [11], a_F being the Thomas-Fermi radius.

It is common to the above approximations that they remove the singularity at $\vartheta = 0$ and predict a finite total scattering cross section on the neutral atom. This is contradictory to the exact numerical calculation of Meyer [12] within the Thomas-Fermi approximation which yields a divergent total scattering cross section on the atom. For scattering in a solid, Meyer also used a finite total scattering cross section. The cutoff radius was set to one-half of the interatomic distance, which exceeds the corresponding cutoff radii of the models [8–11] by an order of magnitude. For the Monte Carlo simulation of RBS spectra, Steinbauer, Bauer, and Biersack [2] varied the cutoff angle by a factor of 10, and within statistical error, found no variation of the total scattering yield. The range of a_c deduced from Ref. [2] is large and includes the values required by the models [8,10,11]. The approximation of a finite cross section on the atom can therefore be used and we shall adopt it for its analytical properties. Its simplest form [8] is given by the cross section (1), with a cutoff at ϑ_c.

B. Determination of the cutoff parameters

An ion penetrating a certain distance into the target is generally deflected by an angle ϑ from its impact direction. The mean value of ϑ is conveniently connected to the mean value of the Legendre polynomials $P_l(\cos\vartheta)$. Due to the addition theorem and the collisional axial symmetry, $\langle P_l(\cos\vartheta_n)\rangle$ after n collisions is related to $\langle P_l(\cos\vartheta_1)\rangle$ after a single collision by [8]

$$\langle P_l(\cos\vartheta_n)\rangle = \langle P_l(\cos\vartheta_1)\rangle^n \quad . \tag{2}$$

Along the ion path, defined by the initial and final energy E_1 and E, respectively, there are on the average ν collisions with target atoms,

$$\nu = \sigma \frac{\rho}{m_1} \int_E^{E_1} \frac{dE}{S(E)} \quad , \tag{3}$$

where σ is the total scattering cross section, ρ the target density, m_1 the target atom mass, and $S(E)$ the ionic stopping power. Assuming Poisson statistics for the particular number of collisions, the mean value of P_l is given by [8]

$$\langle P_l(\cos\vartheta)\rangle = \sum_n e^{-\nu} \frac{\nu^n}{n!} \langle P_l(\cos\vartheta_n)\rangle$$

$$= e^{-\nu[1-\langle P_l(\cos\vartheta_1)\rangle]} \quad . \tag{4}$$

Including (3), the above equation can also be written in the form [13]

$$\langle P_l(\cos\vartheta)\rangle = e^{-\int_E^{E_1} K_l \frac{\rho dE}{S(E)}} \quad , \tag{5}$$

where the parameter K_l is defined by

$$K_l = \frac{1}{m_1} \int \frac{d\sigma}{d\Omega} [1 - P_l(\cos\vartheta)] d\Omega. \tag{6}$$

For the cutoff approximation [8], the values of $\langle P_l(\cos\vartheta)\rangle$ are determined by the angular distribution

$$\frac{dN}{d\cos\vartheta} = \begin{cases} 2\,\frac{1-\cos\vartheta_c}{1+\cos\vartheta_c}\,\frac{1}{(1-\cos\vartheta)^2}, & \vartheta \geq \vartheta_c, \\ 0, & \vartheta < \vartheta_c, \end{cases} \tag{7}$$

which yields

$$\langle \cos\vartheta_1\rangle = 1 + 4\tan^2\left(\frac{\vartheta_c}{2}\right) \ln\left(\sin\frac{\vartheta_c}{2}\right) \approx 1 - \vartheta_c^2 \ln\frac{2}{\vartheta_c},$$

$$\langle P_2(\cos\vartheta_1)\rangle \approx 1 - 3\vartheta_c^2\left(\ln\frac{2}{\vartheta_c} - \frac{1}{2}\right). \tag{8}$$

The approximate part of (8) is valid for small values of ϑ_c. For further work we shall essentially need the value of $\langle P_1(\cos\vartheta)\rangle \equiv \langle\cos\vartheta\rangle$. The corresponding necessary parameter $K_1 \equiv K_c$ is given by [8]

$$K_c = \frac{2\pi d^2}{m_1} \ln\left(1 + \frac{a_c^2}{d^2}\right). \tag{9}$$

It is important to note that the mean values of P_l depend only logarithmically on the total scattering cross section.

The value of a_c was determined by matching the results of (9) with those of the exact numerical integration (6). The integration variable was substituted by the impact parameter b according to the identity $d\sigma = 2\pi b\,db$. The scattering angle ϑ as a function of b was calculated for the Molière potential using the iterative procedure of Biersack and Haggmark [14]. The integration results were found to agree within a few percent with the classical calculation of Janni [13].

For 0.1 MeV protons on Au, the cutoff radius was determined to be $a_c = 0.06$ Å. Using this value in (9) reproduces the result of (6) for $l = 1$ and the data of Janni within ±5% in a rather broad energy interval of 0.05 and 3 MeV (Fig. 1). This implies that a_c is a weak function of energy, which can be ignored within the target.

The model of Andersen *et al.* [11] predicts a similar cutoff radius of 0.067 Å, but the parameter K_1 is then

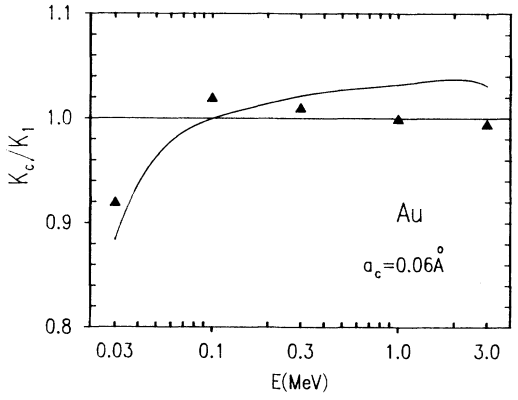

FIG. 1. Comparison of the parameter K_c (9) for proton impact on Au with the numerical results using the iterative procedure [14] (line), and to the classical calculations [13] (triangles).

25% lower than the K_c value of (9). Values closer to (9) would be obtained by a larger Andersen cutoff radius of 0.12 Å.

For $\vartheta \geq \vartheta_c$, the cross section (1) is overestimated with respect to the cross section on the Thomas-Fermi atom [12]. The cutoff at ϑ_c provides an effective value of (1) for the calculation of $\langle \cos\vartheta \rangle$. In the Monte Carlo simulation [2–4], the scattering by angles smaller than ϑ_c was included as an additional correction. This type of correction is now an inherent part of the procedure for the determination of a_c. The cross sections according to the models [10,11] are too low for impact parameters approaching a_c. A correct contribution of the small angle scattering to $\langle \cos\vartheta \rangle$ is then obtained by an increased value of a_c. This effect again supports the use of the cutoff approximation [8] in our work.

C. The single-scattering spectrum

If only single-scattering events contribute to the RBS yield, the spectrum is generally given by [1,15]

$$\frac{d^2N}{dE\,d\Omega}(E) = \frac{d\sigma}{d\Omega}(E')\,N_p\,\frac{\rho}{m_1}\,\frac{dx}{dE} \quad , \tag{10}$$

where E is the energy of scattered ions, $\frac{d\sigma}{d\Omega}$ the Rutherford cross section in the laboratory system [1], N_p the number of ions, and the coordinate x is measured along the incoming beam. The cross section is calculated for the scattering energy E' and should also be corrected for electron screening effects [11]. When calculating the plural- and multiple-scattering corrections to (10), we preferably use the simpler, center of mass cross section (1).

D. The factor of Sirotinin and co-workers

Sirotinin and co-workers [5–7] realized that it is the angular part of the cross section (1) which is most sensitive to plural and multiple scattering. An ion penetrating the target experiences several small-angle and one principal (large-angle) scattering Θ, which is close to the single-scattering angle ψ. A correction factor f was introduced into (10) by averaging the cross section (1) over the angular distribution of incoming and outcoming ions,

$$f = (1-\cos\psi)^2 \times \int d\Omega_i\,d\Omega_o\,\frac{W_i(\vartheta_i,\varphi_i)\,W_o(\vartheta_o,\varphi_o)}{[1-\cos\Theta(\psi,\vartheta_i,\varphi_i,\vartheta_o,\varphi_o)]^2}. \tag{11}$$

Here W_i is the angular distribution of ions after passing the path from the surface to the site of the principal (large-angle) scattering, and W_o is the angular distribution of the ions on the way out. The angles $\vartheta_{i,o}, \varphi_{i,o}$ are measured with respect to the ion trajectory in the single-scattering model. For the evaluation of (11) it was necessary to assume that $W_{i,o}$ are axially symmetric, strongly peaked and nonoverlapping, and that no singularity in the integrand (11) is encountered. The lowest order terms of (11) are

$$f = 1 + \frac{3+\cos\psi}{1-\cos\psi}\,(1-\langle\cos\vartheta_i\rangle + 1-\langle\cos\vartheta_o\rangle) \quad . \tag{12}$$

The authors [5–7] used in (12) a small-angle approximation $1-\langle\cos\vartheta_{i,o}\rangle \approx \frac{1}{2}\langle\vartheta_{i,o}^2\rangle$.

Within the linear approximation already assumed, the general result (12) can be simplified further without significant loss of accuracy. Expanding the right side of (5) up to the linear term we find the relation

$$1-\langle\cos\vartheta_i\rangle + 1-\langle\cos\vartheta_o\rangle \approx \int_{E'}^{E_1} K_1\frac{\rho dE}{S(E)} + \int_{E}^{kE'} K_1\frac{\rho dE}{S(E)} \quad . \tag{13}$$

For heavy targets bombarded by light projectiles, k is close to unity and we can neglect the energy gap between kE' and E'. The integration (13) extends between E and E_1 and yields a linear term for $\langle\cos\vartheta\rangle$ along the entire ion path in the target, but omitting the contribution of the scattering Θ,

$$1-\langle\cos\vartheta_i\rangle + 1-\langle\cos\vartheta_o\rangle \approx \int_{E}^{E_1} K_1\frac{\rho dE}{S(E)} \approx 1-\langle\cos\vartheta\rangle \quad . \tag{14}$$

A comparison of (12) and (14) reveals that the factor f does not essentially depend on the energy of the principal (large-angle) scattering E', which effectively simplifies its evaluation. As shown later in Sec. III, multiplying the single-scattering spectrum (10) by the factor (12) does not fully account for the plural- and multiple-scattering effect.

E. The total-scattering yield

The approximation of a finite scattering cross section allows us to distinguish between ionic trajectories with one, two, and in general n scattering events. The total spectrum $\frac{d^2N}{dE\,d\Omega}$ is the sum of statistically weighted contributions $\frac{d^2N_n}{dE\,d\Omega}$ for particular types of the trajectories. From Sec. II D we may expect that $\frac{d^2N_n}{dE\,d\Omega}$ is proportional to the single-scattering yield $\frac{d^2N_0}{dE\,d\Omega}$. The proportionality factors f_n will be tentatively written as the linear combination

$$f_n = 1 + \sum_{l=1} a_{nl}\,[1-\langle P_l(\cos\vartheta_n)\rangle]. \tag{15}$$

The angular distributions of ions for a not very different number of collisions are similar and we expect that the coefficients a vary slowly with n. Since the probability distribution of scattering events has a distinct maximum at $n \sim \nu$, only a few terms f_n contribute significantly to the total scattering yield. We can therefore discard the n dependence of the coefficients a. This approximation enables an analytic summation of the factors f_n,

$$f = \sum_n e^{-\nu}\,\frac{\nu^n}{n!}\left(1+\sum_l a_l[1-\langle P_l(\cos\vartheta_n)\rangle]\right). \tag{16}$$

The Poisson statistical weights are used as in the calcu-

lation of $\langle \cos\vartheta \rangle$ [8]. Using the relation (2) we find

$$f = 1 + \sum_l a_l (1 - e^{-\nu[1-\langle P_l(\cos\vartheta_1)\rangle]}), \tag{17}$$

and in the linear approximation,

$$f \approx 1 + \nu \sum_l a_l [1 - \langle P_l(\cos\vartheta_1)\rangle]. \tag{18}$$

For low-energy ions and heavy targets, the cutoff approximation [8] predicts ν to be of the order of unity for a large part of the spectrum. The second term in (18) is then essentially the contribution of the double-scattering events multiplied by ν. In the factor f of the Moscow group (12), the summation l contains only the $l = 1$ term, with the coefficient $a_1 = \frac{3+\cos\psi}{1-\cos\psi}$. It may be expected that a more accurate treatment of the double-scattering yield results in an improved correction factor for the plural- and multiple-scattering contribution.

F. The double-scattering process

We shall calculate the spectrum of ions experiencing two scattering events of total scattering angle ψ. Initially we shall assume a constant stopping power and an infinitely heavy target atom ($k = 1$). The ions hit the target surface perpendicularly and the exit beam is inclined at the angle $\pi - \psi$ with respect to the surface normal.

Let us start with the single-scattering spectrum. The ions with exit energy E are scattered by the angle ψ at the target depth x_0,

$$E = E_1 - S x_0 \frac{\cos\psi - 1}{\cos\psi}, \tag{19}$$

which used in (10) gives

$$\frac{d^2N_0}{dE\, d\Omega} = d^2(x_0)\, N_p \frac{\rho}{m_1 S} \frac{|\cos\psi|}{(1-\cos\psi)^3} \quad . \tag{20}$$

For the double-scattering yield, we first attempted to average the cross section (1) over the angular distribution (7). The result was evidently too large by a factor of 2. In a more precise model, the first scattering by an angle ϑ in the azimuthal direction φ appears at the target depth x (Fig. 2). At the distance r from the first scattering event, the second event occurs at an angle Θ. As the ion velocity is now pointing towards the detector, $\cos\Theta = \cos\vartheta\cos\psi + \sin\vartheta\sin\psi\cos\varphi$.

The ions which emerge from the target with energy E (19) travel a path length of the same length. From the geometrical consideration we find

$$E = E_1 - Sx \frac{\cos\psi - 1}{\cos\psi} - Sr \frac{\cos\psi - \cos\vartheta}{\cos\psi} \quad . \tag{21}$$

The number of ions scattered into the solid angle $d\Omega$ is then

$$\frac{dN_1}{d\Omega} = N_p \left(\frac{\rho}{m_1}\right)^2 \frac{d^2(x)}{(1-\cos\vartheta)^2} \frac{d^2(x+r)}{(1-\cos\Theta)^2} \times dx\, dr\, d\cos\vartheta\, d\varphi \quad . \tag{22}$$

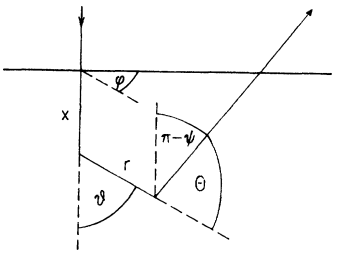

FIG. 2. Geometry of the double-scattering process.

For the energy spectrum we need the number of ions scattered into the energy interval dE. Since it is convenient to integrate over x and $\cos\vartheta$, we express dr by dE (21),

$$dr = \frac{dE\,|\cos\psi|}{S\,|\cos\psi - \cos\vartheta|} \quad . \tag{23}$$

The yield (22) has to be multiplied by $e^{-\nu}$, the probability that there is no other collision on the ion path.

The constants in (22) may be rewritten if we remember that the total cross section and the mean number of scattering events are given by

$$\sigma = \pi a_c^2 = \pi d^2 \frac{1+\cos\vartheta_c}{1-\cos\vartheta_c},$$
$$\nu = \sigma \frac{\rho}{m_1} x_0 \frac{1-\cos\psi}{|\cos\psi|}. \tag{24}$$

As in the derivation of $\langle\cos\vartheta\rangle$ [8], we shall first ignore the energy variation of ϑ_c. An effective value defined at the depth x_0 will be used.

From (22) to (24), the double-scattering spectrum may be expressed as a multiple of the single-scattering spectrum (20),

$$\frac{d^2N_1}{dE\, d\Omega} = \frac{d^2N_0}{dE\, d\Omega} e^{-\nu} \nu g, \tag{25}$$

while the parameter g is given by

$$g = 2|\cos\psi|(1-\cos\psi)^2 \frac{1-\cos\vartheta_c}{1+\cos\vartheta_c} \int \frac{d^2(x)\, d^2(x+r)}{d^4(x_0)} \times \frac{dx\; d\cos\vartheta\; d\varphi}{2\pi x_0 (1-\cos\vartheta)^2 (1-\cos\Theta)^2 |\cos\psi - \cos\vartheta|}. \tag{26}$$

The integral g is of the order of unity. For its evaluation it is necessary to make further approximations. The factor $\frac{d^2(x)\, d^2(x+r)}{d^4(x_0)}$ is a smooth function of x close to unity and can be omitted. Its mean value, estimated for $\vartheta = \frac{\pi}{2}$, exceeds 1.1 for $E < 0.46E_1$. The integration region of (26) is complicated and can best be seen in Fig. 3. It fulfills the two conditions that the path lengths for the exit energy E are appropriately long and that any scattering by an angle smaller than ϑ_c is forbidden. For boundary trajectories, the second scattering occurs at the target surface. In the hatched area of Fig. 3, the azimuthal integration can be performed analytically using the relation

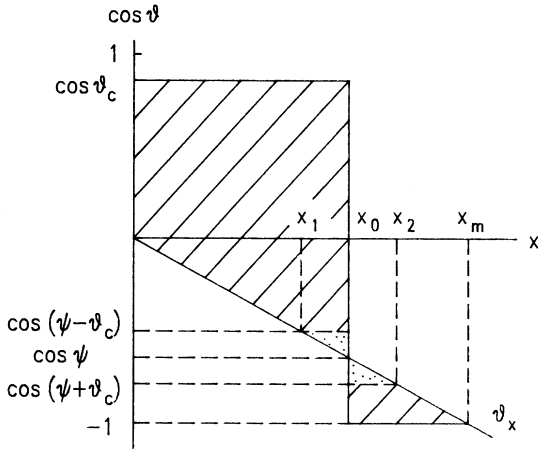

FIG. 3. Integration region for Eq. (26). The ions are scattered up from the depth $x_m = \frac{x_0}{2}\frac{\cos\psi - 1}{\cos\psi}$ and the distances $x_{1,2}$ are given by $x_{1,2} = x_0 \frac{\cos\psi - 1}{\cos\psi}\frac{\cos(\psi \mp \vartheta_c)}{\cos(\psi \mp \vartheta_c) - 1}$. The line ϑ_x is determined by $\vartheta_x = \frac{x\cos\psi}{x_0 - (x_0 - x)\cos\psi}$. There is a logarithmic singularity in the point $(x_0, \cos\psi)$.

$$\frac{1}{2\pi}\int \frac{d\varphi}{(1-\cos\Theta)^2} = \frac{1-\cos\vartheta\cos\psi}{(\cos\vartheta - \cos\psi)^3}. \tag{27}$$

An analytical integration of (26) can be performed in a reasonable way only for $\psi = \pi$ since the integrand is then axially symmetric in the whole integration region. The result is

$$g = \frac{1}{4} + \frac{6\cos\vartheta_c}{(1+\cos\vartheta_c)^3} - \frac{6\cos\vartheta_c}{1+\cos\vartheta_c}\chi\ln\chi + \tfrac{7}{4}\chi - 3\chi^2\ln\chi - \tfrac{9}{4}\chi^2 + \tfrac{1}{4}\chi^3, \tag{28}$$

where we introduced $\chi = \frac{1-\cos\vartheta_c}{1+\cos\vartheta_c}$ to shorten the notation. Since g is a complicated function of ϑ_c we expand it up to the linear term

$$g = 1 + \vartheta_c^2\left(\frac{3}{2}\ln\frac{2}{\vartheta_c} + \frac{5}{8}\right) + \cdots \quad . \tag{29}$$

The expansion (29) is accurate to within 0.5% up to $\vartheta_c = 0.8$. As required by (15), the result (29) is indeed a linear combination of $1 - \langle\cos\vartheta_1\rangle$ and $1 - \langle P_2(\cos\vartheta_1)\rangle$ (8), the coefficients a_l being $\frac{11}{4}$ and $-\frac{5}{12}$, respectively. There is also an agreement between (15) and (25): $g \equiv f_1$.

For $\psi < \pi$, the integration (26) was performed numerically, splitting the integration region into several parts. A new variable $\ln|x - x_0|$ has to be used close to x_0. The integration was Gaussian, with an accuracy of about 0.1%. From (12) it is expected that g depends on ψ predominantly through the factor $\frac{3+\cos\psi}{1-\cos\psi}$. It was found empirically that this factor acts approximately on the term $1 - \langle\cos\vartheta_1\rangle = \vartheta_c^2\ln\frac{2}{\vartheta_c}$, but not on the remaining term $\vartheta_c^2(\frac{1}{2}\ln\frac{2}{\vartheta_c} + \frac{5}{8})$. The factor of $\frac{3}{2}$ in the logarithmic term of (29) is then replaced by $\frac{7+\cos\psi}{2(1-\cos\psi)}$. The validity of this approximation is shown in Fig. 4. The differences between the analytical and numerical values of g are negligible for small values of ϑ_c and for scattering angles close to π, and rise to about 0.6% at $\vartheta_c = 0.3$ and $\psi \sim 145°$.

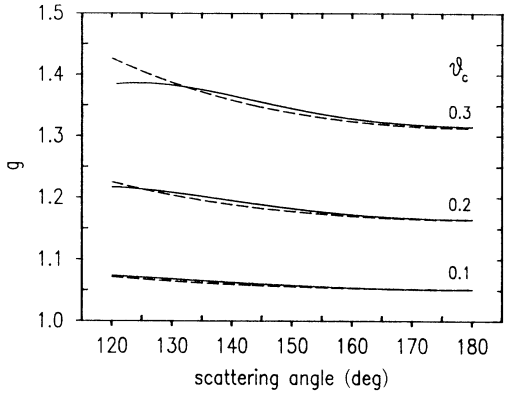

FIG. 4. The factor g (26) calculated numerically as a function of the scattering angle ψ (solid line), and its analytical approximation (29), with the factor of $\frac{3}{2}$ replaced by $\frac{7+\cos\psi}{2(1-\cos\psi)}$ (dashed line).

The factor f (18) is obtained by inserting the right part of (29) into (18). Analogous to (4) and (5), the multiplication by ν in (18) transforms into the integral

$$f = 1 + \frac{2\pi}{m_1}\int_E^{E_1} d^2(E)\left(\frac{7+\cos\psi}{1-\cos\psi}\ln\frac{a_c}{d(E)} + \frac{5}{4}\right)\frac{\rho dE}{S(E)} \quad . \tag{30}$$

Using (6) and (8), the above result may be rewritten in a form which does not necessarily require the cutoff approximation,

$$f = 1 + \frac{19 - 3\cos\psi}{4(1-\cos\psi)}\int_E^{E_1} K_1\frac{\rho dE}{S(E)} - \frac{5}{12}\int_E^{E_1} K_2\frac{\rho dE}{S(E)} \quad . \tag{31}$$

Finally we consider the effect of the kinematic factor k which is smaller than unity. Since for both scattering energies we have not subtracted two short energy intervals, the factors (30) and (31) are slightly overestimated. The resulting error is partly removed if we reduce the upper integration limit E_1 to kE_1. This choice also provides a proper limit of (30) and (31) at the upper energy edge kE_1.

III. RESULTS AND DISCUSSION

Results of the Monte Carlo simulation of 0.1 MeV proton scattering on an Au target [4] served as reference data for the present model (Fig. 5). Proton impact was perpendicular to the target surface and the exit angle was 15° relative to the surface normal. The single-scattering spectrum was calculated from (10). The derivative $\frac{dx}{dE}$ was obtained numerically, by precalculating the tables of E', E, and $\frac{dE}{dx}$ as a function of x. The spectrum height was normalized to the simulated data at the upper en-

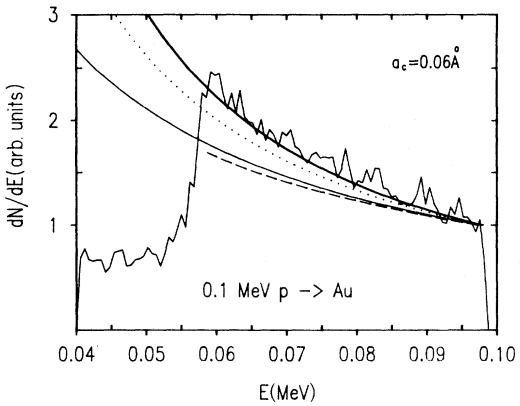

FIG. 5. 0.1 MeV proton backscattering on 1000 Å Au target. The Monte Carlo simulation of Steinbauer *et al.* [4] is shown by a ragged line, and their single-scattering spectrum by a broken line. The single-scattering spectrum according to Eq. (10) is shown by a thin solid line. The dots show the single-scattering spectrum multiplied by the factor of Sirotinin and co-workers (12), and the heavy line by the present factor (30).

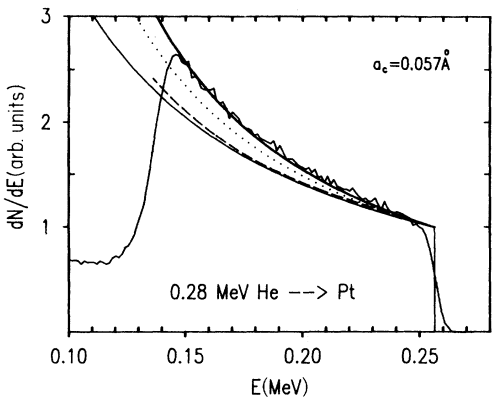

FIG. 6. 0.28 MeV α-particle scattering on 1130 Å Pt target. The ragged line shows the experimental data [1], and the dashed line the original single-scattering spectrum [1]. The other lines are used as in Fig. 5.

ergy edge kE_1. Since statistical fluctuations of the data [4] are quite large, the corresponding value at the energy kE_1 was obtained by a polynomial extrapolation. For low energies, the single-scattering spectrum (10) is a few percent larger than [4]. This difference may be explained by a different approximation for the scattering potential used in the calculation [4] by the TRIM computer program [16].

Multiplying the single-scattering spectrum by the factor of Sirotinin and co-workers (12) does not reproduce the total spectrum generated by the Monte Carlo method [4]. The agreement between the simulated and analytically calculated spectra is considerably improved when the factor f (30) is applied. The difference between the spectra is within the statistical fluctuations [4].

We have also compared the factor (30) to the generalized result (31) which was calculated directly using the iterative procedure [14]. The right terms of (30) and (31) differed by 3% at the lower energy edge, which is within the accuracy of the cutoff approximation (Fig. 1). The resulting difference between (30) and (31) was smaller than 0.7%, and supports the use of the simpler expression (30).

The second example studied is the known case of 0.28 MeV α-particle scattering on Pt [1] (Fig. 6). Here we normalized our data at the upper energy edge of the single-scattering spectrum as given by the authors. For low energies, the calculation (10) yields values somewhat lower than the original single-scattering spectrum. As in the previous case, the factor (12) reproduces about two-thirds of the plural- and multiple-scattering yield, but using the factor (30), a rather good agreement between the calculated and measured spectrum is obtained.

The validity of the present model is limited to light projectiles and heavy targets, and to scattering angles not much different from π and presumably to scattering energies $E \gtrsim \frac{E_1}{2}$. It does not take into account the effect of energy straggling, and only partly considers the inelasticity of the collisions. Since the two effects influence the factor f in an opposite way, they mutually compensate each other. The good results of Figs. 5 and 6 are also supported by the fact that ν does not exceed 1.8 in both cases.

Equation (30) is simple enough to be used routinely in RBS analyzing algorithms. In specific cases some modest fitting of the cutoff radius a_c, or alternatively, of the coefficients a_1 and a_2 (18) should be used. With thin films, there is a spectral contribution below the lower energy edge. Figures 5 and 6 show that the height of this contribution approximately equals the difference between the total and the single-scattering spectrum at the lower energy edge.

IV. CONCLUSION

A simple analytical formula was derived for the thick-target RBS spectrum. The model assumed a finite total scattering cross section on the atom, determined with respect to $\langle \cos \vartheta \rangle$ along the ion path. The double-scattering contribution to the spectrum was found essential for considering trajectories with a higher number of collisions. The total yield was expressed as a multiple of the single-scattering one. The corresponding proportionality factor can be easily included into the existing single-scattering codes.

ACKNOWLEDGMENTS

The author is indebted to Dr. Peter Bauer and to Dr. Erich Steinbauer for helpful discussion and for information about the work of the authors of Refs. [5–7].

[1] W.K. Chu, J.W. Mayer, and M.A. Nicolet, *Backscattering Spectrometry* (Academic, New York, 1978).
[2] E. Steinbauer, P. Bauer, and J. Biersack, Nucl. Instrum. Methods Phys. Res., Sect. B **45**, 171 (1990).
[3] J.P. Biersack, E. Steinbauer, and P. Bauer, Nucl. Instrum. Methods Phys. Res., Sect. B **61**, 77 (1991).
[4] P. Bauer, E. Steinbauer, and J.P. Biersack, Nucl. Instrum. Methods Phys. Res., Sect. B **64**, 711 (1992).
[5] F.G. Neshev, A.A. Puzanov, K.S. Shyshkin, E.I. Sirotinin, A.F. Tulinov, and G.D. Ved'manov, Radiat. Eff. **25**, 271 (1975).
[6] V.Ya. Chumanov, Sh.Z. Izmailov, G.P. Pokhil, E.I. Sirotinin, and A.F. Tulinov, Phys. Status Solidi A **53**, 51 (1979).
[7] E.I. Sirotinin, A.F. Tulinov, V.A. Khodyrev, and V.N. Mizgulin, Nucl. Instrum. Methods Phys. Res., Sect. B **4**, 337 (1984).
[8] S. Goudsmit and J.L. Saunderson, Phys. Rev. **57**, 24 (1940).
[9] G. Wentzel, Z. Phys. **40**, 590 (1927).
[10] K. Güttner, Z. Naturforsch. Teil A **26**, 1290 (1971).
[11] H.H. Andersen, F. Besenbacher, P. Loftager, and W. Möller, Phys. Rev. A **21**, 1891 (1980).
[12] L. Meyer, Phys. Status Solidi B **44**, 253 (1971).
[13] J.F. Janni, At. Data Nucl. Data Tables **27**, 147 (1982).
[14] J.P. Biersack and L.G. Haggmark, Nucl. Instrum. Methods **174**, 257 (1980).
[15] V.I. Roslyakov, A.S. Rudnev, E.I. Sirotinin, A.F. Tulinov, and V.A. Khodyrev, Phys. Status Solidi A **43**, 59 (1977).
[16] E. Steinbauer (private communication).